Rock Mechanics and Rock Engineering (2021) 54:4793–4807
https://doi.org/10.1007/s00603-021-02568-y

ORIGINAL PAPER

Thermal Shock Effect on Acoustic Emission Response During Laboratory Hydraulic Fracturing in Laizhou Granite

Ning Li[1,2] · Shicheng Zhang[2] · Haibo Wang[1] · Shan Wu[2,3] · Yushi Zou[2] · Xinfang Ma[2] · Tong Zhou[1]

Received: 29 March 2021 / Accepted: 30 June 2021 / Published online: 6 July 2021

Abstract

To investigate the thermal shock effect on microseismic response during hydraulic fracturing in hot dry rock, laboratory hydraulic fracturing experiments combined with acoustic emission (AE) monitoring were performed on granite after heating and rapid water-cooling treatments. Thereafter, the influence of thermal treatment level and the number of cycles on hydraulic fracture geometry, injection pressure curve, and the spatial distribution and focal mechanism was analyzed. Besides, the maximum AE amplitude and the localization results of large AE events with amplitudes larger than 7.0 mV were further investigated to discuss the thermal shock effect on reducing breakdown-induced seismicity. Experimental results show that the thermal shock effect was beneficial for reducing the maximum amplitude of AE events during laboratory fracturing experiments on Laizhou granite. After single-cycle thermal treatment, large AE events tended to disperse far away from rather than located around the open-hole section only when the thermal treatment level exceeded the threshold temperature (300 °C). At the thermal treatment level of 300 °C, increasing the number of cycles had a little influence on reducing the breakdown-induced seismicity due to the limited reduction of breakdown pressure. Most of the large AE events are still mainly detected during the occurrence of breakdown and located around the open-hole section. At the thermal treatment level of 400 °C, shear events were dominant. Even though a complex fracture network was created, no obvious cluster of large AE events was detected around the open-hole section.

Keywords Geothermal energy · Hot dry rock · Cyclic thermal shock · Breakdown pressure · Acoustic emission

1 Introduction

Geothermal energy in hot dry rock (HDR) refers to the heat stored in the high-temperature tight crystalline rock mass buried at depths of 3–10 km (Brown 2009; Olasolo et al. 2016; Watanabe et al. 2017; Zhang et al. 2019a). Using hydraulic fracturing to create a large-scale fracture network for the long-term fluid circulation between the injection and production wells is the typical exploitation paradigm of commercial heat extraction from deep HDR formation. This development mode is well known as the enhanced geothermal system (EGS) (Genter et al. 2010; Ghassemi 2012; Breede et al. 2013; Kelkar et al. 2016). Generally, microseismic monitoring is utilized to determine the spatial distribution of created hydraulic fracture network during the stimulation treatment in an injection well. The monitoring results are critical guidance for selecting the location of a production well, so that a successful hydraulic connection can be established. Moreover, the magnitude of microseismic events is also an essential parameter for evaluating the risk of fluid-injection-induced seismicity (Diaz et al. 2018; Zang et al. 2019; Xing et al. 2019; Li et al. 2020). Therefore, understanding the microseismic response during hydraulic fracturing is of great significance for the safe and efficient exploitation of HDR geothermal energy.

As a high-frequency analog of microseismicity, acoustic emission (AE) monitoring has been widely utilized in combination with laboratory hydraulic fracturing (Lockner and Byerlee 1977; Zoback et al. 1977; Stanchits et al. 2009, 2015; Tang et al. 2019). To date, a series of laboratory

✉ Ning Li
lining19900629@163.com

[1] SINOPEC Petroleum Exploration and Production Research Institute, Beijing, China

[2] State Key Laboratory of Petroleum Resource and Prospecting, China University of Petroleum, Beijing, China

[3] Southern University of Science and Technology, Shenzhen, China

hydraulic fracturing experiments on different granites combined with AE monitoring. It has been well acknowledged that the AE monitoring and interpretation technique is conducive to the investigation of dynamic propagation behavior of hydraulic fracture (HF) and the visualization of ultimate fracture geometry (Chitrala et al 2013; Goodfellow et al 2016). Ishida et al. (2000a, 2012, 2013) and Chen et al. (2015) performed a series of laboratory hydraulic fracturing experiments on different granites combined with AE monitoring. Experimental results show that the number of AE events increased, while the breakdown pressure decreased with the increasing of grain size (Ishida et al. 2000a). Compared with water, super-critical or liquid carbon dioxide with lower viscosity was more beneficial for reducing the breakdown pressure and created more complex fracture geometry which was indicated by more three-dimensionally distributed AE events (Ishida et al. 2012, 2013; Chen et al. 2015). Hampton et al. (2017) discussed the damage characterization due to microcracking by comparing the relationship between the density of AE events and the permeability. Hu et al. (2019) performed laboratory fracturing on Sierra White granite under different stress conditions. It was indicated that the higher stress was applied, the more AE events were induced. The focal mechanisms of AE events are generally analyzed to reveal the generation mechanisms of HF. Ishida et al. (2000b) found that shear events dominated in granite specimens with large grain size. Hampton et al. (2013) investigated the focal mechanism of AE events induced in Colorado Rose Red Granite. It was found that shear fractures tended to be dominant when natural fractures or stress concentration exists, while tensile fractures dominate in homogeneous and non-naturally fractured material. Experimental results of Yamamoto et al. (2019) show that the dominant type of AE events is closely related the spatial relationship between the propagated HF and pre-existing weak planes. During stimulation treatments, the radiated seismic energy is also of additional significance. In the previous studies, many parameters have been suggested for further AE analysis (Goodfellow et al. 2016; Ishida et al. 2017; López-Comino et al. 2017). Zhuang et al. (2017, 2018) performed cyclic hydraulic fracturing experiments on core samples of Pocheon granite. Experimental results show that the breakdown pressure in the cyclic injection test was generally reduced by approximately 20% compared with that in monotonic injection tests. Meanwhile, the average value of the induced AE amplitude decreased from 66.3 to 53.3 dB. Diaz et al. (2018) suggested that tensile events mainly induced during the pre-failure period, while more shear events with high energy were monitored during failure/post-failure period.

Even though so many studies have been reported, most of the above-mentioned studies were conducted without consideration of the thermal shock effect. For high-temperature HDR formations, the injection of massive cold water during hydraulic fracturing rapidly cools down the vicinity of wellhole or HF, which induces significant thermal tensile stress (Dusseault 1993; Jansen et al. 1993). Due to this thermal shock effect, inter- and/or intragranular microcracks tend to be created in the wall of the wellbore or perpendicular to the HF surface (Wang et al. 1989; Kumari et al. 2017; Li et al. 2019a, b). Previous experimental results show that the generation of thermally induced microcracks tends to result in significant variation in the physical and mechanical properties of granite, which will further influence the initiation and propagation behavior of HF (Kim et al. 2014; Kumari et al. 2017; Zhao et al. 2018; Wu et al. 2018). Recently, to investigate the thermal shock effect on the hydraulic fracturing process, many laboratory experimental studies have been conducted on granite specimens under high-temperature condition or after pre-heated treatment (Watanabe et al. 2017, 2019; Kumari et al. 2018; Yang et al. 2019; Zhang et al. 2019a, b, c; Li et al. 2020). Experimental results show that the breakdown pressure reduced with the increase of temperature due to the thermally induced mechanical deterioration. Meanwhile, the generation of thermally induced microcracks was also conducive to enhance the complexity of the HF geometry to some extent. However, a few laboratory hydraulic fracturing experiments have been performed combined with AE monitoring in terms of the limitation of equipment in temperature resistance. Consequently, the thermal shock effect on acoustic emission response during laboratory hydraulic fracturing is still not clear yet.

In this study, the thermal shock effect was simulated by heating granite specimens to a series of target temperatures and then rapidly cooled down to room temperature using flowing water. This pre-heating method has been widely used in mechanical tests and laboratory fracturing experiments to investigate the thermal shock effect on mechanical strength and fracture initiation and propagation behavior (Yang et al. 2017, 2019; Zhang et al. 2017; Li et al. 2020). After that, laboratory hydraulic fracturing was performed on pre-heated cuboid granite specimens ($8 \times 8 \times 10$ cm^3) under tri-axial stresses. Meanwhile, the AE activity induced during the experiments was monitored. In the previous study of Li et al. (2020), the fracture initiation and propagation behavior, and the spatial distribution and focal mechanisms of induced AE events in granite specimens after single-cycle thermal treatments have been discussed. In this paper, first, we further focused on the thermal shock effect on the distribution of large AE events which means those with high amplitude (> 7 mV). Based on the obtained new insights, additional laboratory hydraulic fracturing experiments were designed to investigate the cyclic thermal shock effect on fracture geometry, characteristics of the injection pressure curve, and AE response. This study may provide some

references for the exploitation of deep geothermal energy, especially using thermal stimulation.

2 Experimental Method

Large block Laizhou granite was collected from Shandong Province, China. The experimental result of thin section observation shows that the measured grain size mainly ranges from 0.5 to 4.3 mm. X-ray diffraction analysis shows that the granite is composed of quartz 27.5%, potassium feldspar 33.2%, plagioclase 32.0%, calcite 1.8%, mica 4.5%, and clay mineral 1.0%. The porosity and permeability of the virgin granite are 0.7% and 1.9×10^{-3} mD, respectively. The tensile strength of the virgin granite is 11.84 MPa. In the previous study of Li et al. (2020), the temperature dependence of physical and mechanical properties, hydraulic fracture process, and AE response of the Laizhou granite has been investigated after single-cycle thermal treatment. Herein, this paper further illustrated the new insights in the thermal shock effect on AE response from the aspect of AE amplitude. Then, the cyclic thermal shock on mechanical strength, hydraulic fracturing process, and AE response was discussed.

2.1 Specimen Preparation and Cyclic Thermal Treatment

To investigate the cyclic thermal shock effect on tensile strength of Laizhou granite, disc specimens with 2.54 cm in diameter and 1.3 cm in thickness were prepared and then thermally treated as the following procedures: (1) specimens were slowly heated to a series of target temperatures (200 °C, 300 °C, 400 °C, and 500 °C) utilizing a high-temperature furnace at a constant rate of 5 °C/min to avoid the possible thermal shock (Yang et al. 2017; Kumari et al. 2017; Fan et al. 2018); (2) the target temperature was maintained for 4 h to ensure the temperature-equilibrium (Li et al. 2020); (3) the specimens were then rapidly cooled down to room temperature using flowing water to simulate the thermal shock effect during the hydraulic fracturing in HDR (Li et al. 2019a, b); (4) cyclic thermal treatments were performed by repeating steps (1) to (3) for 5, 10, 15, and 20 times, respectively. The scheme of cyclic thermal treatment is shown in Fig. 1. According to the previous experimental results of Li et al. (2020), there exists a threshold temperature of 300 °C for the studies granite, after which the influence of thermal shock on build-up rate and breakdown pressure becomes significant. Therefore, in this study, two target temperatures of 300 °C and 400 °C were selected for cyclic thermal treatments.

Granite specimens for laboratory fracturing experiments were prepared with a dimension of $8\times8\times10$ cm^3. Then, a

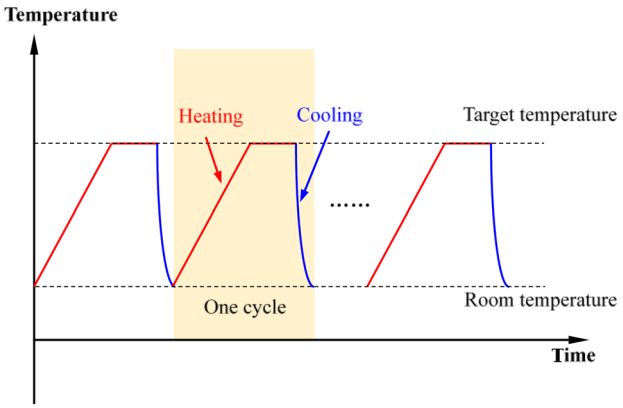

Fig. 1 The scheme of the cyclic thermal treatment (after Wu et al. 2019a, b)

6.5-cm blind hole (i.e., wellhole) with a diameter of 1.5 cm was drilled at the center of an 8×8-cm^2 end face. Thereafter, thermal treatments were performed similarly to the above-mentioned procedures. Noting that the period for thermal equilibrium maintained 8 h for cuboid specimens considering the large specimen size. Additionally, the central hole was intentionally hit during the rapid water-cooling treatment to simulate the thermal shock effect acting on the wall of the wellhole. Considering that the quick evaporation phenomenon of water may block the flow of cold water in the center hole, an injection pipe was inserted into the bottom of center hole, and a constant high injection rate was used when cooling treatment was performed. Compared with drilling the wellhole after thermal treatment, this preparation method is more reasonable to simulate the thermal shock effect in HDR well. In this paper, only the number of cycles of 10 and 20 was considered for laboratory fracturing experiments. After cyclic thermal treatments, as an additional drying process, the granite samples were slowly heated to 60 °C and maintained for 6 h to evaporate the water. Then, a 5.8-cm steel tube (i.e., wellbore) with an external diameter of 1.2 cm was glued into the wellhole using high-strength epoxy, leaving a 2-cm open-hole section at the bottom of the wellhole (Ma et al. 2017a, b; Zou et al. 2017, 2018). Figure 2 shows the granite specimen for laboratory fracturing experiments. Observation results of optical microscope and CT scanning indicated that there existed no visible initial defects in virgin granite specimens, as shown in Fig. 2b,c.

2.2 Laboratory Fracturing Experiment

Laboratory fracturing was performed using a true tri-axial fracturing simulation system, which was composed of a tri-axial loading chamber, a syringe pump, an AE monitoring system, and an injection pressure monitoring system (Ma et al. 2017a, b; Li et al. 2019a, b, c, d). The tri-axial testing

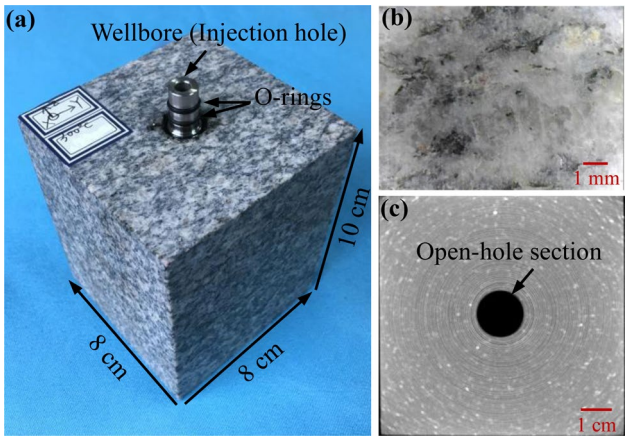

Fig. 2 **a** Granite specimen ($8\times8\times10$ cm^3); **b** surface observation before thermal treatment; **c** CT scanning image cross the open-hole section

system possessed the following capacities: (1) maximum confining stresses of 18 MPa in three directions independently; (2) a maximum injection pressure of 60 MPa; (3) a maximum injection rate of 20 mL/min. In this study, the stress state was set to be 3, 6, and 12 MPa along the X, Y, and Z directions, respectively. Water was used as the fracturing fluid and injected into the wellbore with a constant injection rate of 1 mL/min. The tracer agent (red ink) was added to detect the hydraulic fracture on the specimen surfaces. During the laboratory fracturing, a nine-channel AE monitoring system with an amplitude resolution of 16 bit at 3 MHz sampling rate was used to monitor the AE activity induced by rock failure continuously. The piezoelectric AE sensors (RS-2A) were placed inside the loading plates and arranged on three surfaces according to the principle of maximum volumetric coverage (Frash et al. 2013; Hampton et al. 2013). The frequency range and the resonance frequency of the AE sensors are 50–400 kHz and 150 kHz, respectively. To verify whether these nine sensors arranged on three faces of the specimens were sufficient for AE localization, the pencil lead breaking test was performed. The testing results show that this arrangement scheme is reasonable. The short-time-average/long-time-average (Sta/Lta) method combined with the Akaike information criterion (AIC) method was used to pick the P-wave arrival time (Wu et al. 2017). The characteristic function of the Sta/Lta method is the envelope of AE signal energy getting from Hilbert Transform (Wu et al. 2019a, b). To ensure the reliability of the interpreting results, only those data accepted by more than six sensors were post-processed for analysis of the spatial distribution and hypocenter mechanism of AE events. The Geiger method was introduced to determine the spatial distribution of induced AE events. According to the previous studies, the focal mechanisms/failure modes of AE events were determined by the statistical analysis of P-wave polarity (Lei et al. 1992, 2001; Zang et al. 1998; Bennour et al. 2015; Li et al. 2018b, c; Wu et al. 2019a, b). In this study, according to Li et al. (2018b), the proportion (λ) of dilatational first motions in all well-identified P-wave polarities were used to clarify the tensile ($\lambda<0.3$), shear ($0.3\le\lambda\le0.7$), and compressive events ($\lambda>0.7$). After the experiments, a CT scanning system was utilized to determine the internal fracture distribution (Li et al. 2018a, b). Table 1 shows the detailed experimental parameters for laboratory hydraulic fracturing.

3 Experimental Results Analysis

3.1 Effect of Thermal Shock on Tensile Strength

Figure 3 shows the experimental results of tensile splitting tests of granite specimens after different cyclic thermal treatments. It was shown that the thermal treatment level and the number of cycles had a significant influence on the tensile strength. With the number of cycles increasing from 1 to 20, the tensile strength decreased from 9.02 to 7.59 MPa (by approximately 15.9%) under thermal treatment temperature of 300 °C, while the tensile strength decreased from 8.07 to 4.85 MPa (by approximately 39.9%) under the higher

Table 1 Experimental scheme of laboratory fracturing

Specimen	Temperature (°C)	Cycles number	Stress state (MPa)			Q (mL/min)
			σ_v	σ_h	σ_H	
#1	25	1	12	6	3	1
#2	200	1	12	6	3	1
#3	300	1	12	6	3	1
#4	400	1	12	6	3	1
#5	500	1	12	6	3	1
#6	300	10	12	6	3	1
#7	300	20	12	6	3	1
#8	400	10	12	6	3	1
#9	400	20	12	6	3	1–2

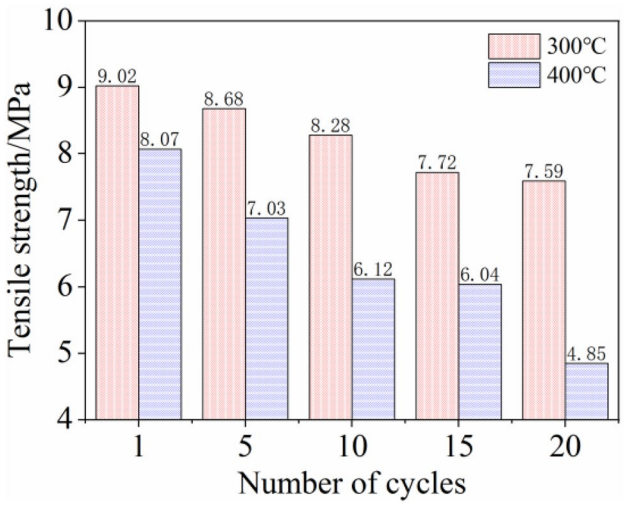

Fig. 3 Variation of tensile strength after thermal treatments: **a** thermal treatment levels; **b** number of cycles

thermal treatment temperature of 400 °C. These experimental results indicate that the cyclic thermal shock effect tends to weaken the mechanical strength of granite more significantly, especially when the thermal treatment temperature was higher than the threshold temperature (300 °C). It can be accounted for by creating more thermally induced microcracks (Kim et al. 2014; Yang et al. 2017; Hu et al. 2018). In our previous study, the obvious damage zone, in which the network of thermally induced microcracks existed, was observed in the wall of open-hole section, especially when the thermal treatment temperatures were higher than 300 °C (Li et al. 2021).

3.2 Effect of Single-Cycle Thermal Shock

Specimens #1 to #5 were fractured after single-cycle thermal treatments. The fracture geometries, injection pressure response, and spatial distribution and focal mechanisms have been thoroughly investigated in the previous study of Li et al. (2020). In this section, additional new insights in the single-cycle thermal shock effect on AE amplitude were aimed to be further discussed. Table 2 summarizes the breakdown pressure (P_b), the maximum amplitude (A_m), and the number of AE events induced in laboratory fracturing experiments. It is worth noting that besides the total number of AE events (N_t), that of AE events with AE amplitude larger than 7.0 mV ($N_{A>7.0}$) was also counted. This criterion was determined out of the consideration that the amplitudes of recorded AE events mainly ranged from 5.0 to 8.0 mV in this study. To intuitively display the spatial localization of the large AE events, the 3D and top view maps were given, as shown in Fig. 4. Particularly, T (blue), S (red), C (black) refer to tensile, shear, and compressive events, respectively.

Table 2 Statistic results of breakdown pressure and AE response after single-cycle thermal shock

Specimen	P_b (MPa)	A_m (mv)	N_t	$N_{A>0}$
#1	14.02	8.15	406	25
#2	13.61	8.23	326	22
#3	13.43	8.24	298	31
#4	11.41	7.82	370	24
#5	8.17	7.55	234	12

Additionally, the size of the spherical ball demonstrated the amplitude of each AE event.

It was indicated that most of the large AE events were located around the open-hole section before 300 °C, as shown in Fig. 4a–c, indicating that the dense clusters of large AE events were closely related to the breakdown. Meanwhile, according to Table 2, the maximum amplitudes of AE events were larger than 8.0 mV for Specimens #1 to #3. When the thermal treatment levels exceeded 300 °C, no cluster of large AE events was induced around the open-hole section and scattered AE events were observed far away from the wellbore in Specimens #4 and #5 (see Fig. 4d, e). It was also worth noting that the maximum amplitude of AE events significantly decreased to 7.82 and 7.55 mV, respectively. The experimental results of the spatial distribution and maximum amplitude of the AE events indicate the potential effect of thermal shock on reducing breakdown-induced seismicity in HDR. As can be seen from Fig. 4 and Table 2, the thermal damage caused by thermal shock tends to prevent the occurrence of large AE events and reduce the largest AE amplitude during the breakdown. In the previous experimental studies of Zhuang et al. (2017, 2018), it was also observed that the maximum amplitude of induced AE hits reduced with the decreasing of breakdown pressure of Pocheon granite. Differently, in the studies of Zhuang et al. (2017, 2018), the effect of cyclic injection scheme was investigated, while this study focused on the thermal shock effect. According to the injection pressure curves reported in our previous study (Li et al. 2020), the thermal shock effect on reducing the risk of breakdown-induced seismicity can be accounted for by the following two mechanisms. For one thing, the breakdown pressure significantly decreased due to the generation of thermally induced microcracks. For another, the degradation rate of the injection pressure after the breakdown was lower, indicating that the input energy was released more slowly.

3.3 Effect of Cyclic Thermal Shock

Although the single-cycle thermal shock was beneficial to reducing the breakdown pressure, the reduction extent was limited (only approximately 5%) before 300 °C (Li et al.,

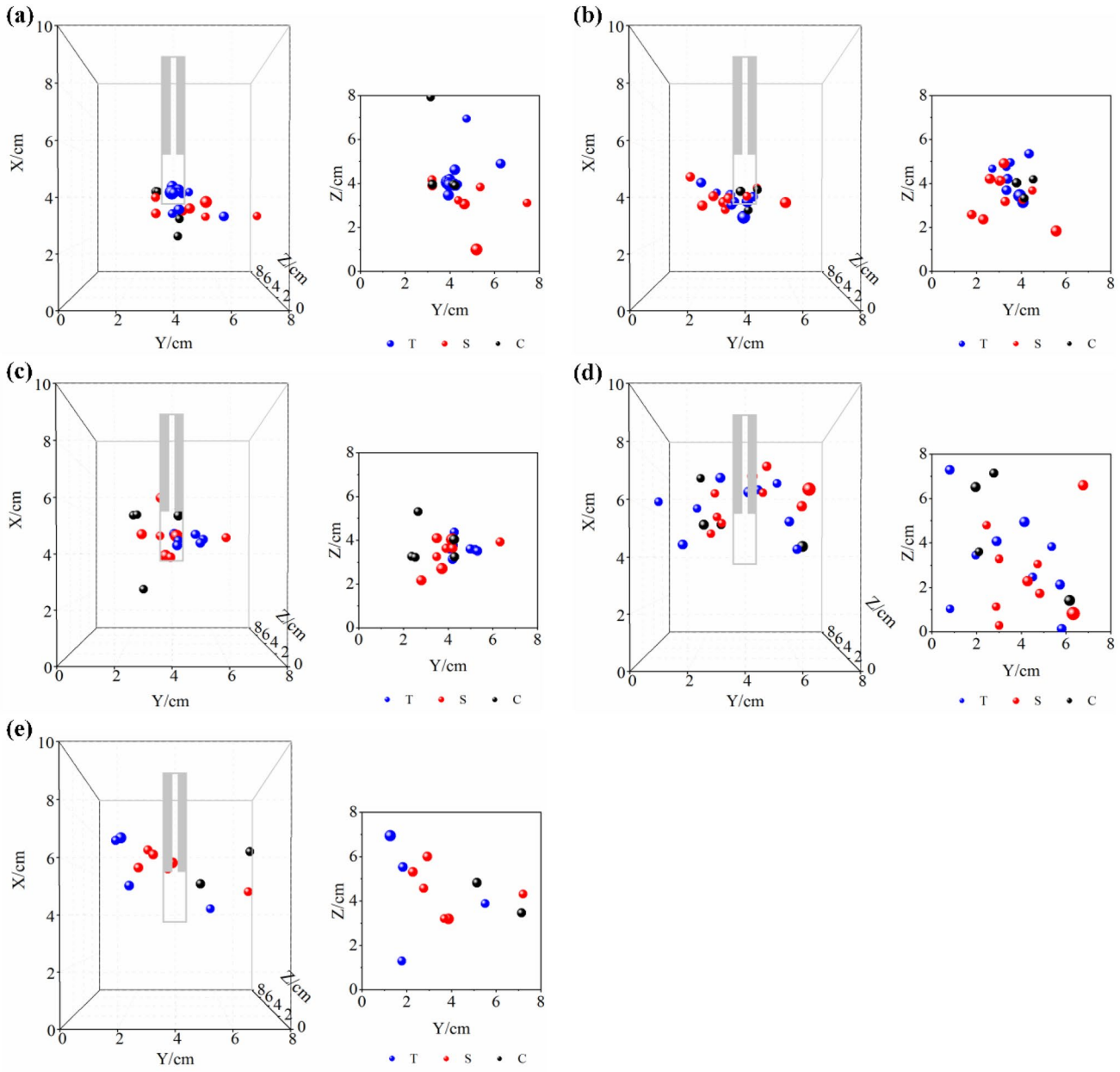

Fig. 4 3D and top views of the spatial distribution of large AE events in granite specimens after single-cycle thermal treatments: **a** Specimen #1–25 °C; **b** Specimen #2–200 °C; **c** Specimen #3–300 °C; **d** Specimen #4–400 °C; **e** Specimen #5–500 °C

2020). According to the results of the mechanical test, it was indicated that increasing the number of cycles of thermal treatments was beneficial for the degradation of tensile strength. Thus, in this section, additional laboratory fracturing experiments were further designed and performed on granite specimens after different cyclic thermal treatments. To discuss the influence of the threshold temperature (300 °C), two target temperatures of 300 and 400 °C were considered.

Figure 5 shows the HF geometries in Specimens #6 and #7 after 10 and 20 cycles of thermal treatments of 300 °C, respectively. An HF initiated from one side of the open-hole section and propagated throughout Specimen #6 (Fig. 5b), while an HF initiated from both sides of the open-hole section and then one wing of the HF terminated in Specimen #7 (Fig. 5e). These asymmetry HF geometries may be corresponding to the inhomogeneous damage induced in the vicinity of the open-hole section. Figure 5c, f shows that the localization of AE events agreed well with the distribution of the HFs. In Specimen #6, all of the AE events were located at the height of the open-hole section and in the left side of the block (Fig. 5c), which in accordance with the

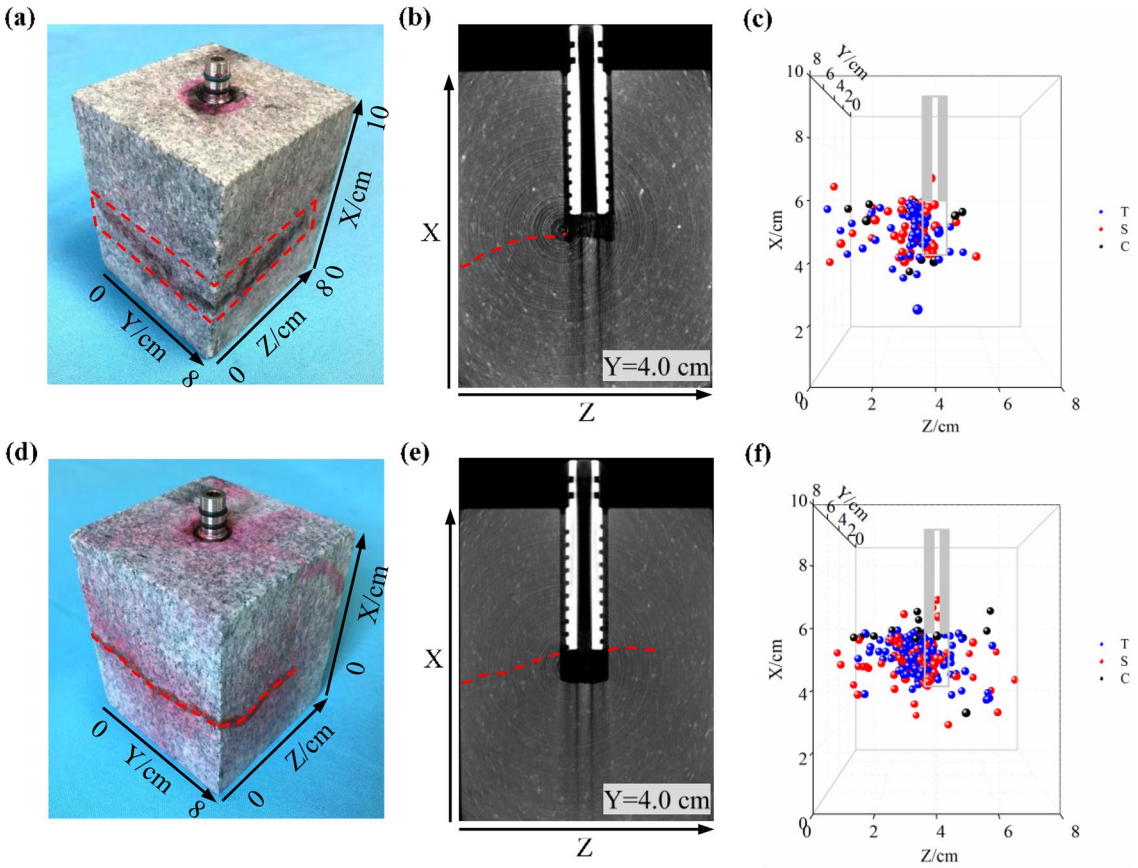

Fig. 5 HF geometry determined by surface observation, CT scanning image, and AE localization in granite specimens after cyclic thermal treatments: **a**–**c** Specimen #6–300 °C × 10; **d**–**f** Specimen #7–300 °C × 20

distribution of the one-wing transverse HF (Fig. 5b). While in Specimen #7, besides the most AE events located in the left side of the block, a few AE events were monitored in the right side (Fig. 5f), indicating the asymmetric propagation of the bi-wing HF (Fig. 5e).

The variation of injection pressure and the recorded AE response versus the injection time (t) during the laboratory fracturing experiments was demonstrated in Fig. 6. As shown in Fig. 6a, after the open-hole was filled with the injected water, the injection pressure of Specimen #6 linearly increased at a build-up rate of 0.071 MPa/s. Then, it was observed that the injection pressure curve slightly deviated from the linear stage at $t = 191$ s. The build-up rate of injection pressure decreased to approximately 0.039 MPa/s. This deviation of injection pressure curve and the following intermittent weak AE activities (< 100 s^{-1}) indicated the initiation of microcracks (Stanchits et al. 2012, 2015; Li et al. 2018a, b, c). The initiation pressure was determined as 11.0 MPa for Specimen #6. At $t = 221$ s, Specimen #6 was finally fractured at a breakdown pressure of 12.81 MPa, which was accompanied by momentary AE activities with high intensity (> 300 s^{-1}). After that, the injection pressure sharply dropped to approximately 0.9 MPa due to the HF propagating throughout the granite specimen. Figure 6b indicates that Specimen #7 underwent similar tendencies in the variation of injection pressure and AE response to that of Specimen #6. Differently, Specimen #7 was linearly pressurized by a lower build-up rate of 0.064 MPa/s at the early stage. Then, microcracks were initiated when the injection pressure reached 10.2 MPa ($t = 173$ s), which was lower than that of Specimen #6. The breakdown pressure of Specimen #7 was 11.83 MPa (approximately 7.5% lower than that of Specimen #6).

Specimens #8 and #9 were prepared by 10 and 20 cycles of thermal treatments at the higher levels of 400 °C, respectively. The characteristics of HF geometries, injection pressure, and AE response are shown in Figs. 7 and 8. It was indicated from the CT scanning images that a single transverse HF (perpendicular to the minimum principal stress) with a tortuous path was created in Specimen #8 (Fig. 7b), while more complex fracture geometry composed of a transverse HF and a longitudinal HF (approximately along the wellbore) was observed in Specimen #9 (Fig. 7e). The enhancement in the complexity of fracture geometry was

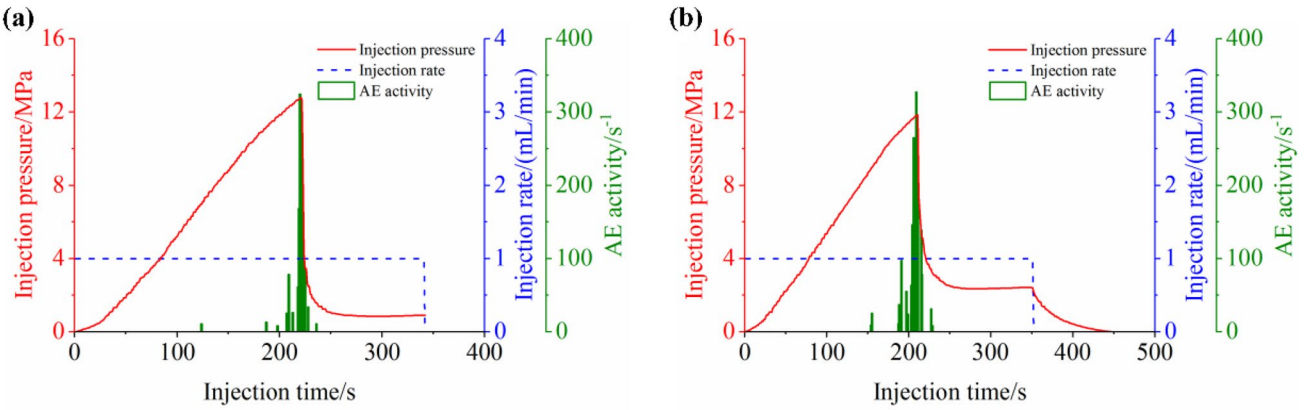

Fig. 6 Injection pressure and AE response during the laboratory fracturing: **a** Specimen #6–300 °C × 10; **b** Specimen #7–300 °C × 20

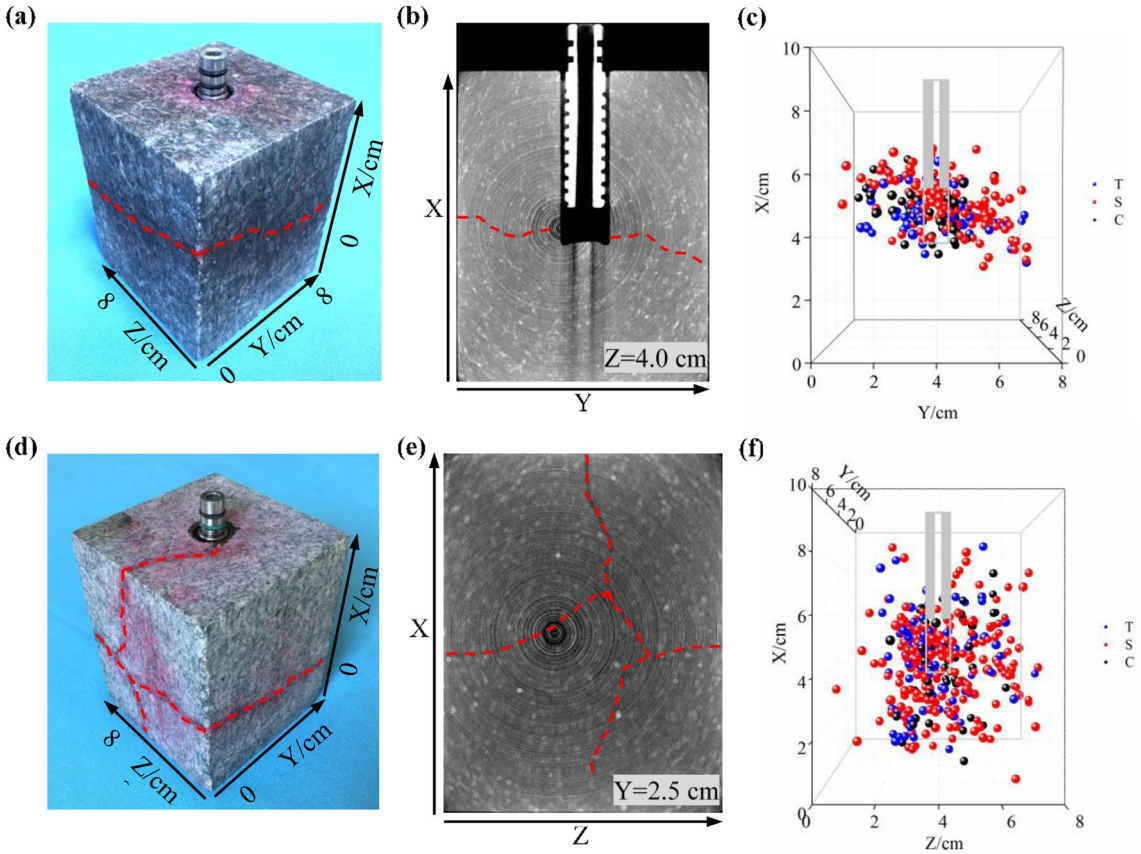

Fig. 7 HF geometry determined by surface observation, CT scanning image, and AE localization in granite specimens after cyclic thermal treatments: **a**–**c** Specimen #8–400 °C × 10; **d**–**f** Specimen #9–400 °C × 20

also well indicated by the spatial distribution of AE events. In Specimen #8, the AE localization results show that the induced AE events were mainly located at the height of the open-hole section and evenly distributed in the both sides of the block (Fig. 7c), indicating the fully propagation of the bi-wing HF. While in Specimen #9, numerous AE events more three-dimensionally distributed (Fig. 7f), which was in accordance with the more complex fracture network, as shown in Fig. 7d.

Figure 8 demonstrates the time dependence of injection pressure curve and AE response during laboratory fracturing experiments on Specimens #8 and #9. As shown in Fig. 8a, the linear build-up (0.046 MPa/s) in the early stage of injection was accompanied by a quiet period of AE activity

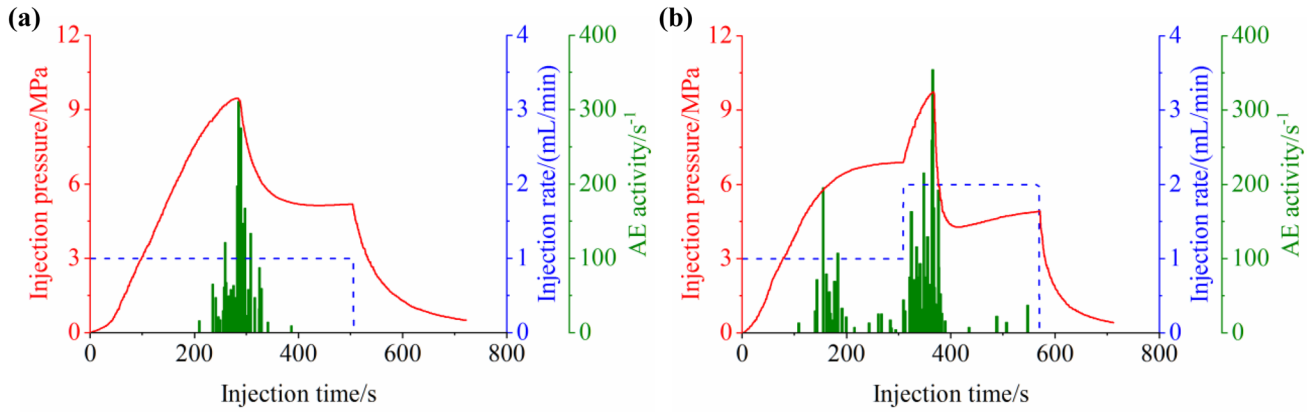

Fig. 8 Injection pressure and AE response during the laboratory fracturing: **a** Specimen #8–400 °C × 10; **b** Specimen #9–400 °C × 20

(t = 45–200 s). When the injection pressure reached 7.6 MPa, a non-linear increase of the injection pressure was observed, and weak AE activities with the intensity of < 100 s^{-1} were simultaneously monitored. At t = 283 s, Specimen #8 was fractured at a breakdown pressure of 9.46 MPa. Meanwhile, the intensity of AE activity reached a peak value of 311 s^{-1}. After that, the injection pressure slowly decreased and then maintained a stable value of 5.1 MPa. The slow dissipation of the injection pressure and the apparent residual pressure may be related to the tortuosity and narrow aperture of the HF caused by the low breakdown pressure. When the laboratory fracturing was performed on Specimen #9, the injection rate was artificially changed according to the injection pressure response, as shown in Fig. 8b. The whole process of injection can be divided into two stages. During the former stage (t = 0–309 s), an injection rate of 1 mL/min was used. First, the injection pressure linearly increased to 4.8 MPa with a build-up rate of 0.044 MPa/s and then non-linearly increased to a stable value of approximately 6.9 MPa. With the occurrence of non-linear build-up (t = 126–220 s), lasting AE activities were monitored, indicating the initiation of microcracks. At t = 310 s, the injection rate was increased to 2 mL/min and maintained constant in the latter stage (t = 310–569 s). Consequently, the injection pressure significantly increased again with a build-up rate of 0.060 MPa/s due to the high injection rate exceeded the fluid leak-off rate. Then, Specimen #9 was fractured at a breakdown pressure of 9.72 MPa (t = 365 s in Fig. 8b), which was followed by a sharp injection pressure drop. Intense AE activities (> 300 s^{-1}) were monitored lasting from the pressurization to the breakdown.

To illustrate the cyclic thermal shock effect on the hydraulic fracturing process, the variation of breakdown pressure and build-up rate with the number of cycles is shown in Fig. 9. It was indicated that the cyclic thermal shock was beneficial for reducing the breakdown pressure of granite, while the reduction extent varies with the thermal treatment level, as shown in Fig. 9a. This agreed well with the variation tendency of tensile strength as shown in Fig. 4. For the thermal treatment level of 300 °C, as the number of cycles increased to 10 and 20, the breakdown pressures decreased from 13.43 to 12.81 and 11.83 MPa (by approximately 5% and 12%), respectively. When the thermal treatment level increased to 400 °C, the breakdown pressure decreased by 17% (from 11.41 to 9.46 MPa) after 10-cycle thermal treatment. At the number of cycles of 20, even though a higher injection rate of 2 mL/min was used, the breakdown pressure (9.72 MPa) was still obviously lower than that after single-cycle thermal treatment.

As shown in Fig. 9b, the variation of build-up rates with the number of cycles indicated that the cyclic thermal shock was conducive to permeability enhancement of Laizhou granite. For 300 °C, the build-up rate of injection pressure linearly decreased from 0.076 to 0.064 MPa/s with the increasing of the number of cycles. While the build-up rate of injection pressure sharply decreased from 0.069 to approximately 0.044 MPa/s for 400 °C. This can be accounted for by the fact that when the thermal treatment level exceeded the threshold temperature, thermal cracking became more significant and more thermally induced microcracks were induced around the wellhole. Additionally, it was worth noting that the degradation extent of the build-up rate during the last ten cycles was obviously smaller than that during the first ten cycles for 400 °C, which indicates that thermal cracking mainly occurred in the early cyclic thermal treatments. A similar conclusion was also reported in the experimental investigation into cyclic thermal shock on mechanical properties of granite (Wu et al. 2019a, b).

Table 3 lists the maximum amplitude (A_m) and total number (N_t) of induced AE events, and the number of large AE events ($N_{A>7.0}$) as well. As shown in Table 3, the maximum amplitude has a positive correlation with the breakdown pressure, indicating that the cyclic thermal shock is helpful for controlling breakdown-induced seismicity. Moreover,

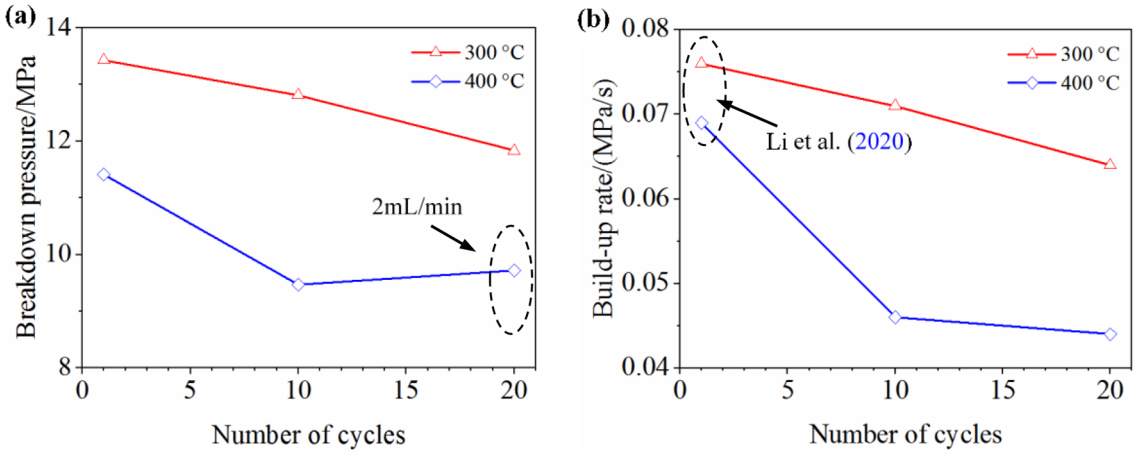

Fig. 9 Influence of cyclic thermal treatment on the characteristic parameters of injection pressure: **a** build-up rate; **b** breakdown pressure

Table 3 Statistic results of AE response after cyclic thermal shock

Specimen	P_b (MPa)	A_m (mv)	N_t	$N_{A>0}$
#6	12.81	8.06	199	23
#7	11.83	7.95	377	20
#8	9.46	7.68	274	36
#9	9.72	7.88	665	69

due to the creation of a complex fracture network, both the total and large AE events induced in Specimen #9 were more than others (see Fig. 7, Table 3). Even though, the maximum amplitudes were lower than 8.0 mV. The statistical analysis results of focal mechanisms of induced AE events are shown in Fig. 10. It was indicated that shear failure mode tended to be dominant owing to the existence of thermally induced microcracks, especially when the thermal treatment level was 400 °C. This experimental result agreed well with the previous studies of Hampton et al. (2013). Additionally, no evident influence of the number of cycles on failure mode was observed in this study.

Figure 11 shows the spatial distribution of large AE events in granite specimens after different cyclic thermal treatments. As shown in Fig. 11a, b, although the number and maximum amplitude of the large AE events after 10- and 20-cycle thermal treatments of 300 °C were smaller compared with those of Specimen #3 (see Tables 2, 3), most of them tended to be induced around the open-hole section. It was indicated that, in this case, increasing the number of cycles has a little influence on reducing the breakdown-induced seismicity due to the limited reduction in tensile strength and breakdown pressure (Figs. 3, 6). Also, it may be related to the release mode of energy during the occurrence of breakdown. As shown in Fig. 6, the injection pressure curves show a sharp pressure drop following the breakdown, which indicated that the

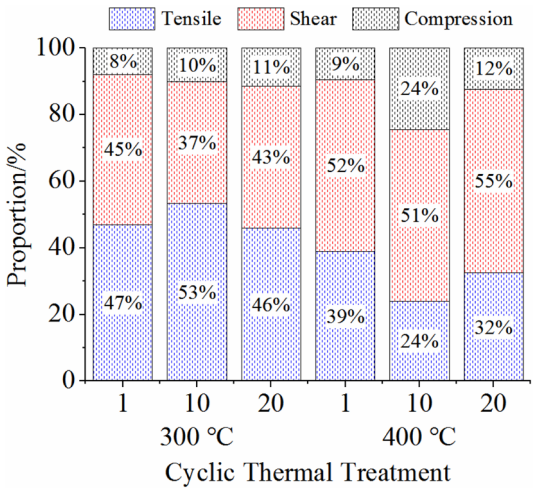

Fig. 10 Statistical analysis of the focal mechanisms of AE events

accumulated elastic energy was quickly released (Stanchits et al. 2015; Li et al. 2018a, b). Figure 11c, d shows the induced large AE events in Specimen #8 and #9 after 10- and 20-cycle thermal treatments of 400 °C, respectively. It was observed that the large AE events mainly dispersed around the location of hydraulic fractures rather than concentrated around the open-hole sections. It should be stressed that the apparent cluster of large AE events in the top view map, in fact, was the projection of those distributed along the longitudinal hydraulic fracture in Specimen #9 (Fig. 11d).

4 Discussion

This experimental study was motivated by the demand of explorating sutable soft stimulation technoque for HDR formation (Zang et al. 2017a, b, 2019; Zhuang et al. 2019).

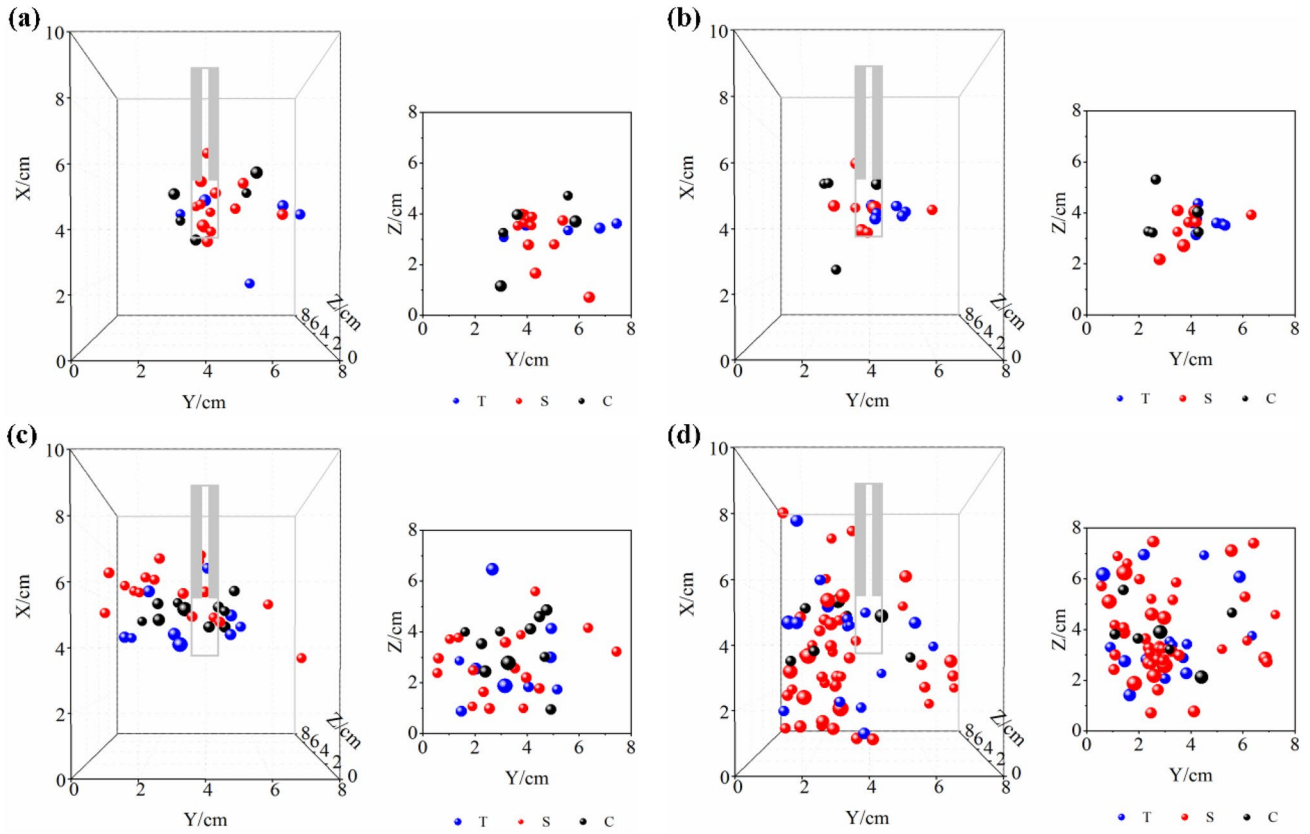

Fig. 11 3D and top views of the spatial distribution of the large AE events: **a** Specimen #6–300 °C×10; **b** Specimen #7–300 °C×20; **c** Specimen #8–400 °C×10; **d** Specimen #9–400 °C×20

Considering the effect of thermal shock on reducing mechanical strength of granite, laboratory hydraulic fracturing experiments were performed on granite after cyclic thermal treatments. Besides the analysis of breakdown prssure, injection pressure curve, and location and focal mechanism of induced AE events, AE amplitude, as a reference value for seismic energy, was also used to evaluate the seismicity during hydraulic fracturing experiments (Li et al. 2018b; Zhuang and Zang 2021). Even though the effect of cyclic thermal shock on reducing the breakdown pressure and the maximum amplitude of AE events was illustrated, there are still some limitations that should be noted.

First, the essence of the thermal shock effect is the thermal stress caused by two mechanisms during the rapid temperature change process: (1) the mismatch in thermal expansion coefficients between adjacent crystalline grains, and (2) the temperature gradient due to the inhomogeneous temerature field. Thus, besides the thermal treatment temerature and the number of cycles, the extent of cyclic thermal shock is also closely related to the heating/cooling rate during the theraml treatment, and the thermal physical and mechanical properties of rock (Finnie et al. 1979; Brotóns et al. 2013). Mechinical tests of different granites showed that the rapid cooling caused more significant sudden thernal shock, resulting in much greater mechanical degradation than that of slow cooling (Kumari et al. 2017; Rossi et al. 2018; Jin et al. 2019). This can be explained by the fact that the higher the convective heat transfer coefficient, the larger the temperature gradient and the thermal stress during heating/cooling treatment process (Wu et al. 2018). It also suggested that the temperature dependence of granite varies with the differences in microstructure and mineral composition, because these microscale characteristics influence the heating transport properties. Experimental results of Zhao (2018) show that the thermal conductivity was negtively correlated with the porosity, while positively correlated with the P-wave velocity and the bulk density. Even though the thermal stress can be induced once the heat transport occurs, only when the thermally induced stresss exceeds the internal strength of the rock matrix, inter-/intra-granular cracks can be initiated. In some studies, different values of threshold temperatures, after which the thermal damage became significant, have been reported for different granite (Li et al. 2020). Thus, further investigations should be continued to fully understand the temperature dependence of granite.

Second, in this study, the large AE events referred to those with AE amplitutes larger than 7.0 mV. This criterion was determined by considering the following two aspects: (1) the threshold value for large AE events were selected as the 70% of the upper limit of AE amplitude which can be recognized by the AE monitoring system; The amplitudes of recorded AE events mainly ranged from 5.0 to 8.0 mV. This threshold value may vary with the experimental conditions and properties of rock, because both tri-axial stress condition and mechanical strength of rock can influence the breakdown pressure, which further influence the AE energy (Zhuang et al. 2017; Xing et al. 2019). Additionally, the size of granite specimens ($8 \times 8 \times 10$ cm^3) was small. According to the time dependence of injection pressure curve and AE activity, most of the induced AE events were induced during the occurrence of breakdown, as shown in Figs. 7 and 9. Therefore, the experimental results only show the effectiveness of thermal shock on reducing the breakdown-induced seismicity. In reality, the experience learn from EGS project sites shows that the existence of a natural fracture network or fault zone is beneficial for achieving the desired heat exchange surfaces (Asanuma et al. 2005; Baisch et al. 2006; Ghassemi 2012; Guo et al. 2019, 2020; Kwiatek et al. 2019; Zhang et al. 2019b). These geological discontinuities have a great influence on the propagation behavior of hydraulic fracture (Yoon et al. 2015; Li et al. 2018a, b, c). It was also suggested that the risk of inducing seismicity is mainly linked to the slippage of large fault zones/natural fractures triggered by water injection (Warpinski et al. 2012; Yong et al. 2015; Zang et al. 2013, 2019; Li et al. 2019a, b, c, d). In addition, in the previous studies of Diaz et al. (2018), it was found that the dominant focal mechanism of AE events transformed from tensile to shear failure mode due to the occrrence of breakdown. In this study, the short process of facture propagation in the small-size specimen makes it difficult to investigate the focal mechanisms change during injection. Thus, to fully understand the thermal shock on the hydraulic fracturing process and induced seismicity, large-scale granite specimens with artificial or natural fractures should be used for laboratory fracturing experiments (Ye et al. 2018, 2019).

5 Conclusion

To investigate the thermal shock effect on characteristics of fracture geometry and AE response, a series of laboratory hydraulic fracturing experiments combined with AE monitoring were performed on Laizhou granite after cyclic thermal treatment. After single-cycle thermal treatment, both the breakdown pressure and the maximum amplitude of induced AE events decrease with the increasing of thermal treatment level. Before 300 °C, a cluster of large AE events (> 7.0 mV) can be observed around the open-hole section, while the large AE events tends to disperses far away from the well bole when the thermal treatment level is higher than 300 °C. Increasing the number of cycles of thermal treatment is helpful to reduce the tensile strength of the studied Laizhou granite. As the number of cycles increases from 1 to 20, the tensile strength decreases by 15.9% and 39.9% after cyclic thermal treatments of 300 °C and 400 °C, respectively, indicating that the higher thermal treatment levels, the higher mechanical degradation extent. Cyclic thermal shock can further reduce the breakdown pressure and the build-up rate of the injection pressure curve due to the generation of thermally induced microcracks. Meanwhile, the complexity of fracture geometry may be improved especially when the thermal treatment level exceeds the threshold temperature (300 °C). At the thermal treatment level of 300 °C, the time dependence of injection pressure and AE activity indicates that the AE events are mainly induced during the breakdown. Even though the maximum amplitude of AE events decreased with the increasing increase of the number of cycles, the large AE events still concentrate around the open-hole section. At the thermal treatment level of 400 °C, shear events dominate ($> 50\%$) according to the focal mechanism analysis. Moreover, although the complex fracture geometry is created after 20-cycle thermal treatments, no obvious cluster of large AE events is induced around the open-hole section.

Acknowledgements This paper was supported by the National Key R&D Program of China (no. 2019YFB1504200) and the SINOPEC Group (no. P19035).

Declarations

Conflict of interest The authors declare no competing financial interest.

References

Bennour Z, Ishida T, Nagaya Y, Chen YQ, Nara Y, Chen Q, Sekine K, Nagano Y (2015) Crack extension in hydraulic fracturing of shale cores using viscous oil, water, and liquid carbon dioxide. Rock Mech Rock Eng 48:1463–1473

Breede K, Dzebisashvili K, Liu X, Falcone G (2013) A systematic review of enhanced (or engineered) geothermal systems: past, present and future. Geoth Energ 1:1–27

Brotóns V, Tomás R, Ivorra S, Alarcón JC (2013) Temperature influence on the physical and mechanical properties of a porous rock: San Julian's calcarenite. Eng Geol 167:117–127

Brown DW (2009) Hot dry rock geothermal energy: important lessons from Fenton Hill. In: 34th workshop on geothermal reservoir engineering

Chen YQ, Nagaya Y, Ishida T (2015) Observation of fractures induced by hydraulic fracturing in anisotropic granite. Rock Mech Rock Eng 48:1455–1461

Chitrala Y, Moreno C, Sondergeld C, Rai C (2013) An experimental investigation into hydraulic fracture propagation under different applied stresses in tight sands using acoustic emissions. J Pet Sci Eng 108:151–161

Diaz M, Jung SG, Zhuang L, Kim KY, Hofmann H, Min KB, Zang A, Zimmermann G, Stephansson O, Yoon JS (2018) Laboratory investigation of hydraulic fracturing of granite under true triaxial stress state using different injection schemes–Part 2. Induced seismicity. In: International conference on coupled processes in fractured geological media: observation, modeling, and application, Wuhan

Dusseault MB (1993) Stress changes in thermal operations. In: SPE international thermal operations symposium. society of petroleum engineers

Fan LF, Gao JW, Wu ZJ, Yang SQ, Ma GW (2018) An investigation of thermal effects on micro-properties of granite by X-ray CT technique. Appl Therm Eng 140:505–519

Finnie I, Copper GA, Berlie J (1979) Fracture propagation in rock by transient cooling. Int J Rock Mech Min Sci Geomech Abstr 16:11–21

Frash LP, Gutierrez M, Hampto J (2013) Scale model simulation of hydraulic fracturing for EGS reservoir creation using a heated true-triaxial apparatus. In: ISRM international conference for effective and sustainable hydraulic fracturing, International Society for Rock Mechanics

Genter A, Evans K, Cuenot N, Fritsch D, Sanjuan B (2010) Contribution of the exploration of deep crystalline fractured reservoir of Soultz to the knowledge of enhanced geothermal systems (EGS). CR Geosci 342(7–8):502–516

Ghassemi A (2012) A review of come rock mechanics issues in geothermal reservoir development. Geotech Geol Eng 30:647–664

Goodfellow SD, Lee B, Flynn W, Maxwell SC, Nasseri MHB, Young RP, Lombos LEA (2016) Acoustic emission geomechanics of hydraulic fracturing in the laboratory. In: The 50th US rock mechanics/geomechanics symposium, Houston, ARMA pp 16–524

Guo T, Gong F, Wang X, Lin Q, Qu Z, Zhang W (2019) Performance of enhanced geothermal system (EGS) in fractured geothermal reservoirs with CO_2 as working fluid. Appl Therm Eng 152:215–230

Guo T, Tang S, Sun J, Gong F, Liu X, Qu Z, Zhang W (2020) A coupled thermal-hydraulic-mechanical modeling and evaluation of geothermal extraction in the enhanced geothermal system based on analytic hierarchy process and fuzzy comprehensive evaluation. Appl Energ 258:113981

Hampton J, Frash L, Gutierrez M (2013) Investigation of laboratory hydraulic fracture source mechanisms using acoustic emission. In: 47th US rock mechanics/geomechanics symposium, American Rock Mechanics Association

Hampton J, Gutierrez M, Matzar L (2017) Damage characterization due to microcracking near coalesced hydraulic fractures with acoustic emission. In: 51st US Rock Mechanics/Geomechanics Symposium, American Rock Mechanics Association

Hu XD, Song XZ, Li GS, Shen ZH, Lyu ZH, Shi Y (2018) Shape factor of the flake-like particle in thermal spallation and its effects on settling and transport behavior in drilling annulus. Powder Technol 335:211–221

Hu LB, Ghassemi A, Pritchett J, Garg S (2019) Characterization of laboratory-scale hydraulic fracturing for EGS. Geothermics. https://doi.org/10.1016/j.geothermics.2019.07.004

Ishida T, Mizuta Y, Matsunaga I, Sasaki S, Chen Q (2000a) Effect of grain size in granitic rock on crack extension in hydraulic fracturing. In 4th North American rock mechanics symposium

Ishida T, Sasaki S, Matsunaga I, Chen Q, Mizuta Y (2000b) Effect of grain size in granitic rocks on hydraulic fracturing mechanism. https://doi.org/10.1061/40514(290)9

Ishida T, Aoyagi K, Niwa T, Chen Y, Murata S, Chen Q, Nakayama Y (2012) Acoustic emission monitoring of hydraulic fracturing laboratory experiment with supercritical and liquid CO_2. Geophys Res Lett 39:L16309. https://doi.org/10.1029/2012GL052788

Ishida T, Nagaya Y, Inui S, Aoyagi K, Nara Y, Chen Y, Chen Q, Nakayama Y (2013) AE monitoring of hydraulic fracturing experiments with CO_2 and water. In: Proceedings of Eurock2013, Wroclaw, Poland, pp 957–962

Ishida T, Labuz JF, Manthei G, Meredith PG, Nasseri MHB, Shin K, Yokoyama T, Zang A (2017) ISRM suggested method for laboratory acoustic emission monitoring. Rock Mech. Rock. Eng. 50(3):665–674

Jansen DP, Carlson SR, Young RP, Hutchins DA (1993) Ultrasonic imaging and acoustic emission monitoring of thermally induced microcracks in Lac du Bonnet granite. J Geophys Res Sol Ea 98(B12):22231–22243

Jin PH, Hu YQ, Shao JX, Zhao GK, Zhu XZ, Li C (2019) Influence of different thermal cycling treatments on the physical, mechanical and transport properties of granite. Geothermics 78:118–128

Kelkar S, WoldeGabriel G, Rehfeldt K (2016) Lessons learned from the pioneering hot dry rock project at Fenton Hill. Geothermics 63:5–14

Kim K, Kemeny J, Nickerson M (2014) Effect of rapid thermal cooling on mechanical rock properties. Rock Mech Rock Eng 47(6):2005–2019

Kumari WGP, Ranjith PG, Perera MSA, Chen BK, Abdulagatov IM (2017) Temperature-dependent mechanical behavior of Australian Strathbogie granite with different cooling treatments. Eng Geol 20:31–44

Kumari WGP, Ranjith PG, Perera MSA, Li X, Li LH, Chen BK, Avanthi Isaka BL, De Silva VRS (2018) Hydraulic fracturing under high temperature and pressure conditions with micro CT applications: geothermal energy from hot dry rocks. Fuel 230:138–154

Kwiatek G, Saamo T, Ader T, Bluemle F, Bohnhoff M, Chendorain M, Dresen G, Heikkinen P, Kukkonen I, Leary P, Leonhardt M, Malin P, Martínez-Garzón P, Passmore K, Passmore P, Valenzuela S, Wollin C (2019) Controlling fluid-induced seismicity during a 61-km-deep geothermal stimulation in Finland. Sci Adv 5:eaav7224

Lei XL, Nishizawa O, Kusunose K, Satoh T (1992) Fractal structure of the hypocenter distributions and focal mechanism solutions of acoustic emission in two granites of different grain sizes. J Phys Earth 40(6):617–634

Lei XL, Kusunose K, Rao MVMS, Nishizawa O, Satoh T (2001) Quasi-static fault growth and cracking in homogeneous brittle rock under triaxial compression using acoustic emission monitoring. J Geophys Res 105(B3):6127–6139

Li N, Zhang SC, Zou YS, Ma XF, Wu S, Zhang YN (2018a) Experimental analysis of hydraulic fracture growth and acoustic emission response in a layered formation. Rock Mech Rock Eng 51(4):1047–1062

Li N, Zhang SC, Zou YS, Ma XF, Zhang ZP, Li SH, Chen M, Sun YY (2018b) Acoustic emission response of laboratory hydraulic fracturing in layered shale. Rock Mech Rock Eng 51(11):3395–3406

Li YW, Rui ZH, Zhao WC, Bo YH, Fu CK, Chen G, Patil P (2018c) Study on the mechanism of rupture and propagation of T-type fractures in coal fracturing. J Nat Gas Sci Eng 52:379–389

Li N, Zhang SC, Ma XF, Zou YS, Cao T (2019a) Experimental research on the effect of cold water injection on the mechanical properties and brittleness of granite in HDR. In: 53rd US rock mechanics/geomechanics symposium, American Rock Mechanics Association

Li N, Zhang SC, Ma XF, Li SH, Zhang ZP, Zou YS (2019b) Temperature-dependency of mechanical properties of hydraulic fracture surface and its influence on conductivity: an experimental study

for development of geothermal energy. In: ARMA-CUPB Geothermal International Conference, American Rock Mechanics Association

Li SH, Zhang SC, Ma XF, Zou YS, Li N, Chen M, Cao T, Bo ZK (2019c) Hydraulic fractures induced by water-/carbon-dioxide-based fluids on tight sandstones. Rock Mech Rock Eng. https://doi.org/10.1007/s00603-019-01777-w

Li TY, Gu Y, Wang ZZ, Wang RJ, Chen YF, Song T-A, Wang RH (2019d) Spatiotemporal variations in crustal seismic anisotropy surrounding induced earthquakes Near Fox Creek, Alberta. Geophys Res Lett. https://doi.org/10.1029/2018GL081766

Li N, Ma XF, Zou YS, Wu S, Li SH, Zhang ZP, Cao T (2020) Thermal effects on the physical and mechanical properties, and fracture initiation of Laizhou granite during hydraulic fracturing. Rock Mech Rock Eng 53:2539–2556

Li N, Zhang SC, Wang HB, Ma XF, Zou YS, Zhou T (2021) Effect of thermal shock on laboratory hydraulic fracturing in Laizhou granite: an experimental study. Eng Fract Mech 248:107741

Lockner D, Byerlee JD (1977) Hydrofracture in Weber sandstone at high confining pressure and differential stress. J Geophys Res Atmos 82(14):2018–20265

López-Comino JA, Cesca S, Heimann S, Grigoli F, Milkereit C, Dahm T, Zang A (2017) Characterization of hydraulic fractures growth during the ¨Asp¨o hard rock laboratory experiment (Sweden). Rock Mech Rock Eng 50:2985–3001

Ma XF, Li N, Yin CB, Li YC, Zou YS, Wu S, He F, Wang XQ, Zhou T (2017a) Hydraulic fracture propagation geometry and acoustic emission interpretation: A case study of Silurian Longmaxi Formation shale in Sichuan Basin, China. Petrol Explor Dev 44(6):974–981

Ma XF, Zou YS, Li N, Chen M, Zhang YN, Liu ZZ (2017b) Experimental study on the mechanism of hydraulic fracture growth in a glutenite reservoir. J Struct Geol 97:37–47

Olasolo P, Juarez MC, Morales MP, Amico DS, Liarte IA (2016) Enhanced geothermal systems (EGS): a review. Renew Sust Energy Rev 56:133–144

Rossi E, Kant MA, Madonna C, Saar MO, Rohr PRV (2018) The effects of high heating rate and high temperature on the rock strength: feasibility study of a thermally assisted drilling method. Rock Mech Rock Eng 51:2957–2964

Stanchits S, Fortin J, Gueguen Y, Dresen G (2009) Initiation and propagation of compaction bands in dry and wet Bentheim sandstone. Pure Appl Geophys 166(5):843–868

Stanchits S, Burghardt J, Surdi A (2015) Hydraulic fracturing of heterogeneous rock monitored by acoustic emission. Rock Mech Rock Eng 48(6):2513–2527

Stanchits S, Surdi A, Edelman E, Suarez-Rivera R (2012) Acoustic emission and ultrasonic transmission monitoring of hydraulic fracture initiation and growth in rock samples. In: The 30th European Conference on Acoustic Emission Testing & 7th International Conference on Acoustic Emission, Granada, Spain

Tang J, Ehlig-Economides C, Fan B, Cai B, Mao W (2019) A microseismic-based fracture properties characterization and visualization model for the selection of infill wells in shale reservoirs. J Nat Gas Sci Eng 67:147–159

Wang HF, Bonner BP, Carlson SR, Kowallis BJ, Heard HC (1989) Thermal stress cracking in granite. J Geophy Res Sol Earth 94:B2. https://doi.org/10.1029/JB094iB02p01745

Warpinski NR, Du J, Zimmer U (2012) Measurements of hydraulic-fracture-induced seismicity in gas shales. SPE Prod Oper 27:240–252

Watanabe N, Numakura T, Sakaguchi K, Saishu H, Okamoto A, Ingebritsen SE, Tsuchiya N (2017) Potentially exploitable supercritical geothermal resources in the ductile crust. Nat Geosci 10:140–144

Watanabe N, Sakaguchi K, Goto R, Miura T, Yamane K, Ishibashi T, Chen Y, Komai T, Tsuchiya N (2019) Cloud-fracture networks as a means of accessing superhot geothermal energy. Sci Rep 9:939. https://doi.org/10.1038/s41598-018-37634-z

Wu S, Ge HK, Wang XQ, Meng FB (2017) Shale failure processes and spatial distribution of fractures obtained by AE monitoring. J Nat Gas Sci Eng 41:82–92

Wu XG, Huang ZW, Li R, Zhang SK, Wen HT, Huang PP, Dai XW, Zhang CC (2018) Investigation on the damage of high-temperature shale subjected to liquid nitrogen cooling. J Nat Gas Sci Eng 57:284–294

Wu S, Li TT, Ge HK, Wang XQ, Li N, Zou YS (2019a) Shear-tensile fractures in hydraulic fracturing network of layered shale. J Petrol Sci Eng 183:106428

Wu XG, Huang ZW, Cheng Z, Zhang SK, Song HY, Zhao X (2019b) Effects of cyclic heating and LN_2-cooling on the physical and mechanical properties of granite. Appl Therm Eng 156:99–110

Xing YK, Zhang GQ, Luo TY, Jiang YW, Ning SW (2019) Hydraulic fracturing in high-temperature granite characterized by acoustic emission. J Petrol Sci Eng 178:475–484

Yamamoto K, Naoi M, Chen Y, Nishihara K, Yano S, Kawakata H, Akai T, Kurosawa I, Ishida T (2019) Moment tensor analysis of acoustic emissions induced by laboratory-based hydraulic fracturing in granite. Geophys J Int 216:1507–1516

Yang SQ, Ranjith PG, Jing HW, Tian WL, Ju Y (2017) An experimental investigation on thermal damage and failuremechanical behavior of granite after exposure to different high temperature treatments. Geothermics 65:180–197

Yang RY, Huang ZW, Shi Y, Yang ZQ, Huang PP (2019) Laboratory investigation on cryogenic fracturing of hot dry rock under triaxial-confining stresses. Geothermics 79:46–60

Ye Z, Ghassemi A (2018) Injection-induced shear slip and permeability enhancement in granite fractures. J Geophys Res Solid Earth 123:9009–9032

Ye Z, Ghassemi A (2019) Injection-induced propagation and coalescence of preexisting fractures in granite under triaxial stress. J Geophys Res Solid Earth 124:7806–7821

Yoon JS, Zimmermann G, Zang A, Stephansson O (2015) Discrete element modeling 985 of fluid injection–induced seismicity and activation of nearby fault. Can Geotech J 52(10):1457–1465

Zang A, Wagner FC, Stanchits S, Dresen G, Andresen R, Haidekker M (1998) Source analysis of acoustic emissions in Aue granite cores under symmetric and asymmetric compressive loads. Geophys J Int 135:1113–1130

Zang A, Yoon JS, Stephansson O, Heidbach O (2013) Fatigue hydraulic fracturing by cyclic reservoir treatment enhances permeability and reduces induced seismicity. Geophys J Int 195(2):1282–1287

Zang A, Stephansson O, Stenberg L, Plenkers K, Specht S, Milkereit C, Schill E, Kwiatek G, Dresen G, Zimmermann G, Dahm T, Weber M (2017a) Hydraulic fracture monitoring in hard rock at 410 m depth with an advanced fluid-injection protocol and extensive sensor array. Geophys J Int 208(2):790–813

Zang A, Stephansson O, Zimmermann G (2017b) Keynote: fatigue hydraulic fracturing. In: ISRM European rock mechanics symposium, EUROCK 191, pp 1126–1134

Zang A, Zimmermann G, Hofmann H, Stephansson O, Min KB (2019) How to reduce fluid-injection-induced seismicity. Rock Mech Rock Eng 52:475–493

Zhang F, Zhao JJ, Hu DW, Skoczylas F, Shao JF (2017) Laboratory investigation on physical and mechanical properties of granite after heating and water-cooling treatment. Rock Mech Rock Eng 51(3):677–694

Zhang YJ, Ma YQ, Hu ZJ, Lei HL, Bai L, Lei ZH, Zhang Q (2019a) An experimental investigation into the characteristics of hydraulic

fracturing and fracture permeability after hydraulic fracturing in granite. Renew Energy 140:615–624

Zhang W, Guo TK, Qu ZQ, Wang ZY (2019b) Research of fracture initiation and propagation in HDR fracturing under thermal stress from meso-damage perspective. Energy 178:508–521

Zhang W, Qu Z, Guo T, Wang Z (2019c) Study of the enhanced geothermal system heat mining from variably fractured hot dry rock under thermal stress. Renew Energy 143:855–871

Zhao XG, Zhao Z, Guo Z, Cai M, Li X, Li PF, Chen L, Wang J (2018) Influence of thermal treatment on the thermal conductivity of Beishan Granite. Rock Mech Rock Eng 51:2055–2074

Zhuang L, Zang A (2021) Laboratory hydraulic fracturing experiments on crystalline rock for geothermal purposes. Earth Sci Rev 2016:103580

Zhuang L, Kim KY, Jung SG, Nam YJ, Min KB, Park S, Zang A, Stephansson O, Zimmermann G, Yoon JS (2017) Laboratory evaluation of induced seismicity reduction and permeability enhancement effects of cyclic hydraulic fracturing. In: 51st US rock mechanics/geomechanics symposium, American Rock Mechanics Association

Zhuang L, Kim KY, Jung SG, Diaz M, Min KB, Park S, Zang A, Stephansson O, Zimmermann G, Yoon JS (2018) Cyclic hydraulic fracturing of cubic granite samples under triaxial stress state with acoustic emission, injectivity and fracture measurements. In: 52nd US rock mechanics/geomechanics symposium, American Rock Mechanics Association

Zhuang L, Kim KY, Jung SG, Diaz M, Min KB, Zang A, Stephansson O, Zimmermann G, Yoon JS, Hofmann H (2019) Cyclic hydraulic fracturing of pocheon granite cores and its impact on breakdown pressure, acoustic emission amplitudes and injectivity. Int J Rock Mech Min Sci 122. https://doi.org/10.1016/j.ijrmms.2019.104065

Zoback MD, Rummel F, Jung R, Raleigh CB (1977) Laboratory hydraulic fracturing experiments in intact and pre-fractured rock. Int J Rock Mech Min Sci Gemech Abstr 14(2):49–58

Zou YS, Ma XF, Zhou T, Li N, Chen M, Li SH, Zhang YN, Li H (2017) Hydraulic fracture growth in a layered formation based on fracturing experiments and discrete element modeling. Rock Mech Rock Eng 50:2381–2359

Zou YS, Li N, Ma XF, Zhang SC, Li SH (2018) Experimental study on the growth behavior of supercritical CO_2-induced fractures in a layered tight sandstone formation. J Nat Gas Sci Eng 49:145–156